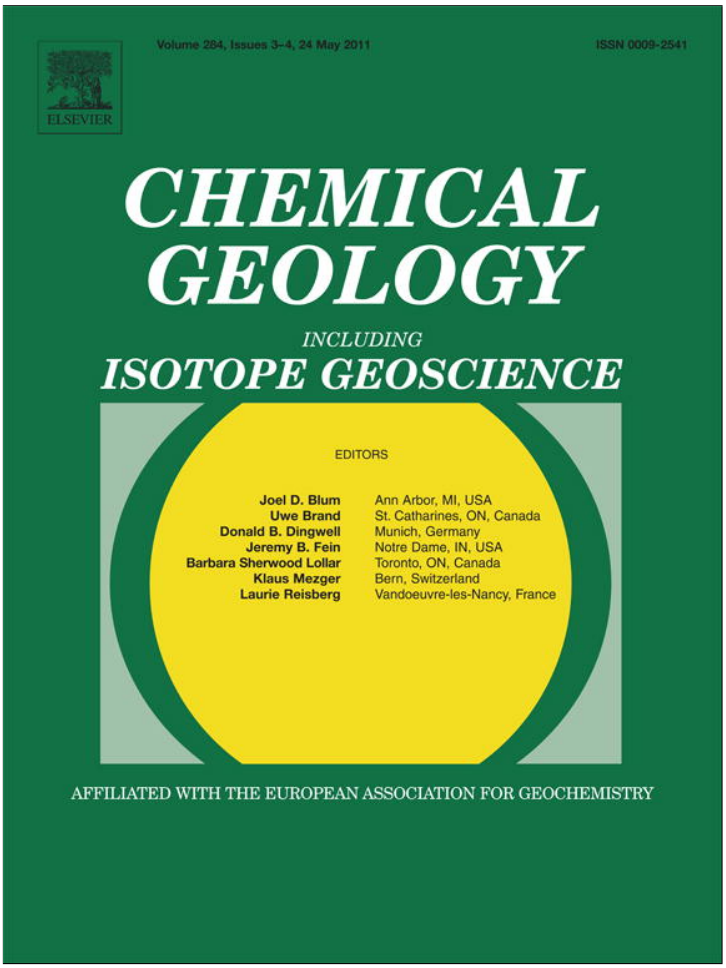

Chemical Geology 284 (2011) 333–338

Contents lists available at ScienceDirect

Chemical Geology

journal homepage: www.elsevier.com/locate/chemgeo

Research paper

Experimental determination of the phase boundary between kornelite and pentahydrated ferric sulfate at 0.1 MPa

W.G. Kong [a,b,*], Alian Wang [b], I-Ming Chou [c]

[a] School of Physics, Shandong University, Jinan 250100, China
[b] Department of Earth and Planetary Sciences and McDonnell Center for Space Sciences, Washington University, St. Louis, MO 63130, USA
[c] 954 National Center, U.S. Geological Survey, Reston, VA 20192, USA

ARTICLE INFO

Article history:
Received 2 November 2010
Received in revised form 17 March 2011
Accepted 17 March 2011
Available online 25 March 2011

Editor: J. Fein

Keywords:
Hydrous ferric sulfates
Experiment
Kornelite
Pentahydrate
Phase boundary

ABSTRACT

Recent findings of various ferric sulfates on Mars emphasize the importance of understanding the fundamental properties of ferric sulfates at temperatures relevant to that of Martian surface. In this study, the phase boundary between kornelite ($Fe_2(SO_4)_3 \cdot 7H_2O$) and pentahydrated ferric sulfate ($Fe_2(SO_4)_3 \cdot 5H_2O$) was experimentally determined using the humidity-buffer technique together with gravimetric measurements and Raman spectroscopy at 0.1 MPa in the 36–56 °C temperature range. Through the thermodynamic analysis of our experimental data, the enthalpy change (-290.8 ± 0.3 kJ/mol) and the Gibbs free energy change (-238.82 ± 0.02 kJ/mol) for each water molecule of crystallization in the rehydration of pentahydrated ferric sulfate to kornelite were obtained.

1. Introduction

Hydrous ferric sulfates have been found by the two Mars Exploration Rovers (MER), and the dehydration of ferric sulfate (after the exposure to current Mars surface atmospheric conditions) at one site has been suggested by MER data analysis (Wang and Ling, 2011). Among the hydrous ferric sulfates found on Mars, only jarosite ($(K,Na,H_3O)Fe_3(SO_4)_2(OH)_6$) has been definitively identified, in the Meridiani outcrop using Mössbauer spectrometry (MB) (Klingelhöfer et al., 2003, 2004). The presence of other types of ferric sulfates is indicated by the MB spectral analysis of the light-toned salty soils exposed by the Spirit rover at several sites in the Gusev Crater (Morris et al., 2006, 2008). On the basis of a spectral deconvolution study of the Vis–NIR spectra extracted from the Pancam multicolor images (Bell et al., 2003), ferricopiapite ($Fe^{3+}_{4.67}(SO_4)_6(OH)_2 \cdot 20H_2O$) was identified as the major ferric sulfate phase at three sites in Gusev where light-toned salty soils were excavated, with hydronium jarosite ($(H_3O)Fe^{3+}3(SO_4)_2(OH)_6$), fibroferrite ($Fe^{3+}(SO_4)(OH) \cdot 5H_2O$), rhomboclase ($HFe^{3+}(SO_4)_2 \cdot 4H_2O$), and paracoquimbite ($Fe_2(SO_4)_3 \cdot 9H_2O$) as coexisting minor phases (Johnson et al., 2007). Moreover, a property change of light-toned salty soils excavated from the depth at Tyrone site in Gusev was observed through seven consecutive Pancam observations after these soils were exposed to the Martian surface atmospheric conditions (Wang et al., 2008a). The dehydration of ferricopiapite accounts for the observed change on the basis of the stability field and the phase transition pathway of ferricopiapite and a comparison with the standard spectra of various ferric sulfates (Wang and Ling, 2011). At a broader scale, iron sulfates have been identified from orbit by the CRISM Vis–NIR spectrometer (Mars Reconnaissance Orbiter). These sulfates include szomolnokite ($FeSO_4 \cdot H_2O$) at the Juventae Chasma (Bishop et al., 2009), jarosite within the Mawrth Vallis region (Farrand et al., 2009), ferric sulfates (possibly copiapite group) in the East Candor and the Capri Chasma (Roach et al., 2007), and a ferric sulfate hydroxide ($Fe^{3+}(SO_4)(OH)$) at the Aram Chaos (Lichtenberg et al., 2010).

The finding of iron sulfates on Mars has stimulated many experimental and theoretical studies about their fundamental properties (Chipera et al., 2007; Freeman et al., 2009; Ling et al., 2008; Ling and Wang, 2010; Tosca et al., 2007; Wang et al., 2008b; Xu et al., 2009). Among these properties, establishing the phase boundaries between various ferric sulfates in the temperature range relevant to Mars is essential for understanding the occurrence of the ferric sulfates and their phase transitions on Mars.

On Earth, ferric sulfates are common oxidation products of pyrite or other sulfide minerals. The oxidation process of iron sulfides can produce iron- and sulfate-rich solutions of low pH from which hydrated iron sulfates can precipitate. These processes have been

* Corresponding author at: School of Physics, Shandong University, Jinan 250100, China.
E-mail address: gavink@levee.wustl.edu (W.G. Kong).

0009-2541/$ – see front matter © 2011 Elsevier B.V. All rights reserved.
doi:10.1016/j.chemgeo.2011.03.014

observed in the acid mine drainage systems (e.g. Buckby et al., 2003; Jambor et al., 2000; Nordstrom et al., 2000). The release of toxic metals during this oxidation process reported (Nordstrom and Alpers, 1999) reinforces the significance of understanding the ferric sulfates system in the terrestrial environment.

The solubility relationships of the minerals in the Fe_2O_3—SO_3—H_2O system were experimentally investigated in the 50–200 °C temperature range by Posnjak and Merwin (1922), and referred by Williams (1990). Using the quadruple points determined in the experiments (i.e., two coexisting solid phases in contact with related solution and vapor), Posnjak and Merwin (1922) also derived the phase diagram for the Fe_2O_3—SO_3—H_2O system in the 50–200 °C temperature range. Combining the solubility data with those reported by Wirth and Bakke (1914) at 25 °C, Merwin and Posnjak (1937) extrapolated the solubility relationship of the system into a lower temperature range, 30–40 °C, without giving the phase boundary. Their estimations are approximately consistent with the experimentally determined solubility curves at 25 °C reported by Baskerville and Cameron (1935).

The observed temperatures on the Mars surface (during medium obliquity period) in the equatorial region are generally below 20 °C (Kieffer et al., 1977; Schofield et al., 1997; Smith et al., 2004; Spanovich et al., 2006), thus the phase diagram for the Fe_2O_3—SO_3—H_2O system at low temperature range (<50 °C) is needed. In preliminary experiments, we studied the stability fields and phase transition pathways among several ferric sulfates in the 5–50 °C temperature range (Wang et al., 2010). On the basis of those experiments, we have designed new experimental procedures to determine the phase boundaries among several pairs of ferric sulfates. This work reports the phase boundary between kornelite ($Fe_2(SO_4)_3\cdot 7H_2O$, 7w) and pentahydrated ferric sulfate ($Fe_2(SO_4)_3\cdot 5H_2O$, 5w).

Our experimental approach is to apply a humidity-buffer technique, gravimetric measurements, and Raman spectroscopy to determine two points on the phase boundary in the T–RH (temperature–relative humidity) space between kornelite and pentahydrated ferric sulfate at 0.1 MPa in the 36–56 °C temperature range. We then calculate the enthalpy change and the Gibbs free energy change for each water molecule of crystallization in the rehydration of pentahydrated ferric sulfate to kornelite as well as the phase boundary between the two ferric sulfates. Finally, we compared our experimentally derived standard Gibbs free energy of reaction (ΔG_r^0) and standard enthalpy of reaction (ΔH_r^0) with those reported in the literature.

2. The kornelite–pentahydrated ferric sulfate system

We chose kornelite (7w) and pentahydrated ferric sulfate (5w) as the first pair in our phase boundary study because of the simplicity of their phase transition, neutral to neutral, with two structural water molecules transferred. Kornelite has been found in the copper queen mine in Arizona (Merwin and Posnjak, 1937), while there is no natural terrestrial occurrence of pentahydrated ferric sulfate to our knowledge. Although insignificant on Earth compared with other ferric sulfates species, the experimental determination of their phase boundary and the derived thermodynamic constants will (1) help to evaluate and confirm the results of their solubility between 50 and 200 °C as reported by Posnjak and Merwin (1922); (2) help to evaluate the previously reported thermodynamic data, which were either determined experimentally with the calorimetric technique or estimated (Ackermann et al., 2009; Hemingway et al., 2002; Majzlan et al., 2006); and (3) establish a methodology for determining the phase boundaries of other ferric sulfates using the RH buffer technique, the gravimetric measurements and the Raman Spectroscopy.

In the structure of kornelite, three water molecules are coordinated with each Fe to form an octahedron, and each octahedron shares three oxygen atoms with three SO_4 tetrahedra to form parallel layers (Robinson and Fang, 1973). The remaining one structural water molecule is bonded between these layers through hydrogen bonding. In the crystal structure of pentahydrated ferric sulfate, Fe occurs at two octahedral sites, $[Fe(OH_2)_3O_3]$ and $[Fe(OH_2)_2O_4]$ (Majzlan et al., 2005).

The reaction involved in the phase transition between kornelite and pentahydrated ferric sulfates is:

$$Fe_2(SO_4)_3\cdot 7H_2O_{(s)} \leftrightarrow Fe_2(SO_4)_3\cdot 5H_2O_{(s)} + 2H_2O_{(g)} \quad (1)$$

where s refers to a solid state and g a gas state.

The thermodynamic relation for this reaction is:

$$\Delta G_r^0 = -RT\ln K = -2RT\ln(f_{H2O}/0.1) = -2RT\ln\left[(f^*_{H2O}/0.1)(\%RH)/100\right] \quad (2)$$

where ΔG_r^0 is the standard Gibbs free energy of reaction; K is equilibrium constant for the reaction; R is gas constant (8.31451 J/mol K); T is absolute temperature; f_{H2O} is equilibrium H_2O fugacity (in MPa); and f^*_{H2O} is the fugacity of pure H_2O at liquid–gas equilibrium (in MPa). The standard states for minerals and H_2O are pure solids and H_2O gas, respectively at 0.1 MPa and temperature. By determining the equilibrium relative humidity ($\%RH$) or equilibrium water fugacity (f_{H2O}) at different temperatures, the Gibbs free energy of reaction and the equilibrium constant for this reaction can be derived.

3. Experiments

In our experiments, we use a humidity-buffer technique (Chou et al., 2002) to obtain the equilibrium RH between kornelite and pentahydrated ferric sulfate in the 35–56 °C temperature range at 0.1 MPa. Along the humidity buffer curves reported by Greenspan (1977), Reaction (1) will change direction (either dehydration or rehydration) after going through the point where a RH buffer curve intersects with the phase boundary. This direction change is revealed by gravimetric measurements on the samples (mixtures of kornelite and pentahydrated ferric sulfate). We use Raman spectroscopy to provide phase identifications, including the identity of potential unexpected phases resulting from the complicated phase transition pathways of ferric sulfates (Chipera et al., 2007; Jerz and Rimstidt, 2003; Posnjak and Merwin, 1922; Wang et al., 2010).

We used the mixture of kornelite (7w) and pentahydrated ferric sulfate (5w) as the starting material. These two ferric sulfates were synthesized using the methods reported by Ling and Wang (2010). The mixture (200–400 mg) of the sulfates was loaded in an open glass vial (8 mm internal diameter and 30 mm tall). The vial was partially immersed in a humidity-buffer solution in a larger glass vial (15 mm internal diameter and 45 mm tall) that was tightly caped and sealed by Teflon tape. The humidity-buffer solutions were saturated salt solutions of NaBr and KI that buffered the RH of the vapor in the head space of the buffer vial. The RH levels were controlled by the temperature of the salt solution (Greenspan, 1977; Chou et al., 2002). The sealed RH buffer vial (that contains an open small vial loaded with the mixture of 7w and 5w ferric sulfates) was immersed in a water bath (Neslab RTE-110 by Thermo Fisher) having a temperature stability of ±0.1 °C. The temperature of the water bath was measured using a Pt resistance probe with an accuracy of ±0.1 °C. The ferric sulfate mixtures in the small open sample vial were directly in contact with the vapor in the head space of the RH buffer vial. This geometry allowed the mixture of kornelite and pentahydrated ferric sulfate to react with the vapor phase under well defined RH and a well controlled temperature. Experiments were run for durations of 48–120 h to produce mass change of the mixture large enough to determine the direction of Reaction (1). The gravimetric measurements of the sample vials were made using a balance (METTLER AE100 by METTLER TOLEDO Inc.) with precision of ±0.1 mg (Table 1).

Table 1
Experimental results at 0.1 MPa (the mean of bolded temperatures was taken as the equilibrium temperatures).

Humidity buffer	T (°C)	Starting mass (mg)	Duration (h)	Mass change (mg)
KI	55.5	358.5	120	6.2
	56	416.7	96	**1.7**
	56.4	416.4	120	**−0.3**
	57	269.9	96	−0.2
	58	337.2	120	−2.3
NaBr	34.3	281.5	48	0.2
	35.2	229.8	96	0.2
	35.6	231.2	72	**0.2**
	36	229.9	72	**−0.1**
	36.4	231.4	96	−0.1
	39.8	282.9	72	−1.4

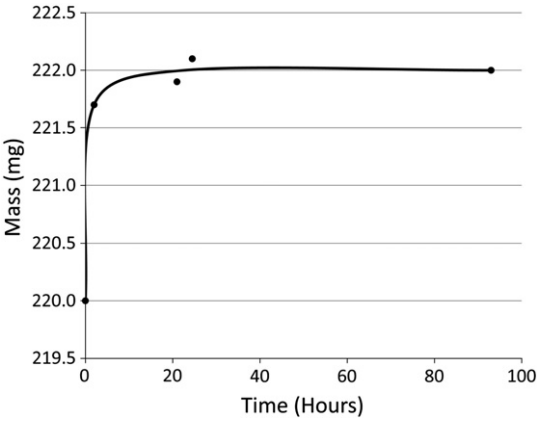

Fig. 1. Water absorption rate of pentahydrated ferric sulfate powder in KI RH buffer at room temperature (20 °C). The sample mass changes quickly in the first few hours before reaching the saturation of adsorbed water at about 24 h.

We did not seek the total conversion of the mixture to either 7w or 5w, which can take thousands of hours (Wang et al., 2010). Instead, we used the direction of Reaction (1) determined at one T–RH point by gravimetric measurement to select the temperature setting of the next experiment, i.e., to increase T (by one step) when rehydration was found or to decrease T (by one step) when dehydration was found. For each RH buffer (NaBr or KI), a large T step was used initially within a large T range (e.g., $\Delta T = 8$ °C in the 8–48 °C temperature range). The magnitude of the T steps was gradually reduced with decreased T ranges as the target T was approached (e.g., $\Delta T = 2$ °C in the 32–40 °C temperature range and $\Delta T = 0.4$ °C in the 34–36.4 °C temperature range). A total of 16 independent experiments were conducted in order to find the 7w–5w phase boundary point on the NaBr buffer curve. The same procedure was used to find the 7w–5w phase boundary point on the KI buffer curve.

We used multi-point Raman measurements to check the identity of starting phases and the experimental products as the Raman technique can identify minor and trace phases in a mixture (Wang et al., 2005, 2006). For the Raman measurements, a small amount of sample powder was placed on a glass slide and pressed slightly with another slide to have a flat surface. On that flat surface, 20–100 Raman spectra were obtained for each sample using automatic Raman line scan. All Raman spectra were collected using a KOSI (Kaiser Optical Systems Inc.) HoloLab5000-532 laser Raman spectrometer. The Raman spectrometer uses the 532 nm line of a frequency-doubled Nd:YAG laser as the excitation source and it covers the spectral range of 4000–100 cm^{-1} with a spectral resolution of 4–5 cm^{-1}. The wavelength of the Raman spectrometer was calibrated using a neon emission lamp. The spectral intensity was corrected against a secondary intensity standard tungsten lamp calibrated at KOSI. The laser wavelength was checked each working day using the Raman peak of a Si standard at 520.7 cm^{-1} at 20 °C, and was corrected to be within ± 0.2 cm^{-1}. The wavelength accuracy and precision were found to be better than 0.1 cm^{-1} in the spectral region of interest, as determined by the spectral peak fitting using the GRAMS-32 AI software.

We recognize that the mass change observed in our sample mixtures can be caused by two effects: (1) by the gain and loss of the adsorbed water on the surface of mineral grains, and (2) by the dehydration or rehydration of hydrous ferric sulfates. In general, the amount of adsorbed water at the surface of mineral grains can change when the environmental RH level or the temperature surrounding the sample changes. In the experiments studying the $MgSO_4 \cdot 6H_2O \leftrightarrow MgSO_4 \cdot 4H_2O$ phase boundary by Chou and Seal (2007), the mass change caused by losing one H_2O molecule is about 7.9 wt.% of the total mass of $MgSO_4 \cdot 6H_2O$, thus the mass change caused by dehydration/rehydration was relatively easy to be distinguished from that caused by the change of adsorbed water. In our experiments examining the $Fe_2(SO_4)_3 \cdot 7H_2O \leftrightarrow Fe_2(SO_4)_3 \cdot 5H_2O$ phase boundary, the mass change caused by losing one H_2O molecule in the total mass of kornelite is only 3.4 wt.%. Compared to the study of Mg-sulfates, it is more difficult to distinguish the mass change caused by dehydration/rehydration from that caused by the change of adsorbed water. In order to remove this uncertainty, we devised a special procedure to prepare our starting ferric sulfate samples. The individual starting samples (7w or 5w) were put into an environment with RH and T values close to the values of estimated phase boundary, but within their own stability field for more than 72 h, in order to reach the saturation of adsorbed water (e.g., Fig. 1). The amount of adsorbed water of pentahydrated ferric sulfate increased very quickly in the first few hours before reaching the saturation of adsorbed water in less than 24 h (Fig. 1). We used multi-point Raman measurements (>20 spots) to check each starting phase (7w or 5w) after this procedure, in order to examine the purity and homogeneity of the starting phases. By preparing the starting 7w and 5w material in this way, the observed mass change caused by dehydration or rehydration was distinguished from the mass change caused by adsorbed water.

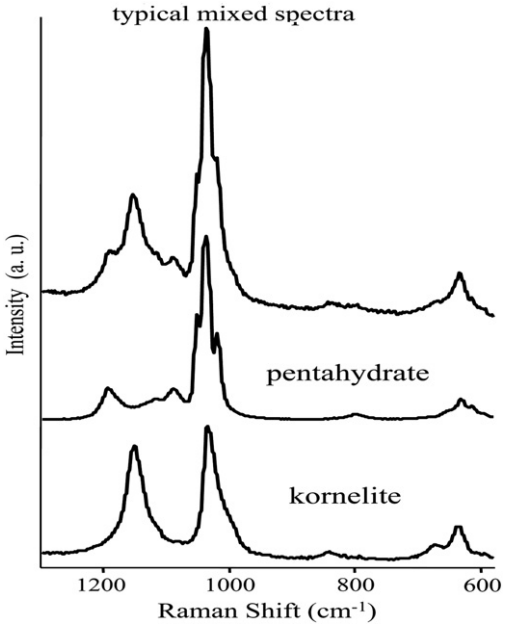

Fig. 2. Raman spectra of the synthetic pure phases (kornelite and pentahydrated ferric sulfate) and a typical experimental product as mixture.

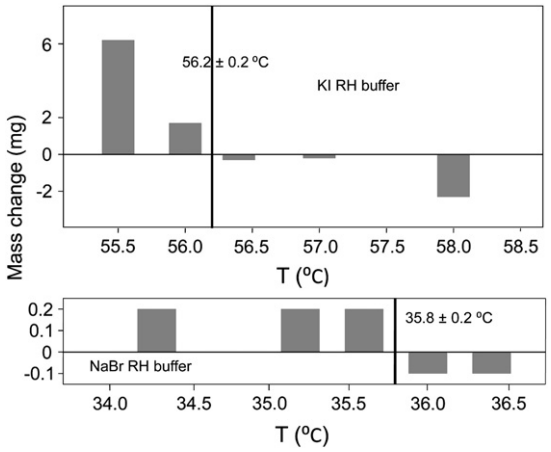

Fig. 3. Experimental results showing mass changes of 7w–5w mixtures developed with the KI-saturated (top) and NaBr-saturated (bottom) aqueous solutions as RH buffers at fixed temperatures. Mass increase suggests rehydration of 5w in mixture, thus a T below the 7w–5w phase boundary. Mass decrease suggests the dehydration of 7w in mixture, thus a T above the 7w–5w phase boundary. The equilibrium temperatures at 7w–5w phase boundary, marked by the heavy vertical lines, were bracketed by the directional mass changes.

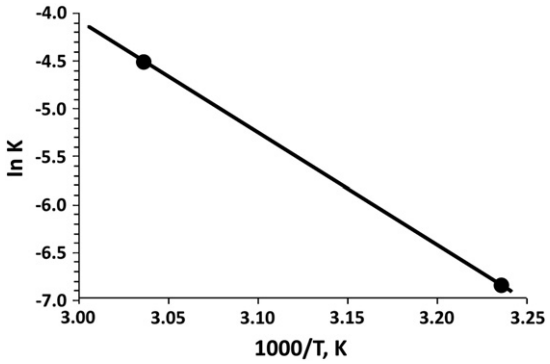

Fig. 4. The ln K vs. 1/T plot for the 7w–5w equilibria at 0.1 MPa. The dots represent equilibrium points at 56.2 and 35.8 °C along KI and NaBr humidity buffer curves, respectively.

4. Results

In all of our experiments (Table 1), only Raman spectra of kornelite, pentahydrated ferric sulfate, and the mixture of these two phases were encountered in the starting materials and products (Fig. 2). The two equilibrium points on the 7w–5w phase boundary are located at 35.8 ± 0.2 °C and 54.32 ± 0.06% RH along the NaBr buffer, and at 56.2 ± 0.2 °C and 63.62 ± 0.03% RH along the KI buffer (Fig. 3). We calculated the RH values at these two temperatures from the data of Greenspan (1977) and we calculated the equilibrium constants from Eq. (2) (Table 2; Fig. 4), and can be represented by:

$$\ln K(\pm 0.02) = -11773/T + 31.243 \quad (3)$$

Values of f^*_{H2O} (MPa, Table 2) were calculated from the equations of Haar et al. (1984). The value of ΔG^0_r at 298.15 K was calculated from Eq. (2), and the standard enthalpy of reaction, ΔH^0_r, was calculated using the van't Hoff relation (Table 3):

$$\partial(\ln K)/\partial(1/T) = -\Delta H^0_r/R \quad (4)$$

The value of the entropy of reaction, ΔS^0_r, was calculated from the relation (Table 3):

$$\Delta G^0_r = \Delta H^0_r, -T\Delta S^0_r \quad (5)$$

Using these thermodynamic parameters, we derived the phase boundary between kornelite and pentahydrated ferric sulfate in a RH–T space (Fig. 5).

5. Discussion

Using a different approach, Ackermann et al. (2009) have estimated the phase boundary between kornelite and pentahydrated ferric sulfate. They used the enthalpies of formation from elements for pentahydrated ferric sulfate (−4115.8 ± 4.1 kJ/mol, $Fe_2(SO_4)_3 \cdot 5H_2O$, Majzlan et al., 2006) and kornelite (−4916.2 ± 4.2 kJ/mol, $Fe_2(SO_4)_3 \cdot 7.75H_2O$, Ackermann et al., 2009), which they measured employing a calorimetric technique, to calculate the standard enthalpy for reaction (1), ΔH^0_r. Then they sketched two different phase boundaries for kornelite and pentahydrated ferric sulfate using the two different entropies of reaction (1), ΔS^0_r, which they estimated. However, one of their 7w–5w phase boundaries intersects with 273 K at 145% RH, and the other at 17% RH. The locations of their predicted 7w–5w phase boundaries are inconsistent with the observation of Posnjak and Merwin (1922), where $Fe_2(SO_4)_3 \cdot 6H_2O$ (a crystal structure refinement study suggested to be pentahydrated (5w), Majzlan et al., 2005) was found to be stable above 50 °C (333 K). In addition, these locations (Ackermann et al., 2009) are far from the stability fields of kornelite (7w) and pentahydrated ferric sulfate (5w) established experimentally by Wang et al. (2010), in which, 5w was found to be stable at 34% RH in the 5–50 °C range for $>2\times10^4$ h. The uncertainties in their estimations of ΔS^0_r and the propagated uncertainties in their calculations of ΔG^0_r should account for the unreasonable locations of the derived phase boundaries reported by Ackermann et al. (2009). On the other hand, the phase boundary derived from our experiments is consistent with the experimental observations of Posnjak and Merwin (1922) and Wang et al. (2010).

Nevertheless, it is worth to compare the thermodynamic parameters for this ferric sulfate phase transition derived from our experimental results with those derived from calorimetric measurements (Ackermann et al., 2009; Majzlan et al., 2006) and those derived using humidity buffer technique on other iron sulfates (Chou et al., 2002). Note all these parameters are calculated at 298.15 K and at 0.1 MPa.

The enthalpy change for each water of crystallization ($\Delta H^\circ_{xw,\,298.15K}$) and the Gibbs free energy change for each water of crystallization ($\Delta G^\circ_{xw,\,298.15K}$) at 298.15 K can be calculated from the results of this experimental study for reaction (1):

$$\Delta H^\circ_{xw,298.15K} = -\left(\Delta H^\circ_{r,298.15K} - n\Delta H^\circ_{f,H2O,298.15K}\right)/n \quad (6)$$

$$\Delta G^\circ_{xw,298.15K} = -\left(\Delta G^\circ_{r,298.15K} - n\Delta G^\circ_{f,H2O,298.15K}\right)/n \quad (7)$$

where n = 2; $\Delta H^\circ_{r,\,298.15K}$ and $\Delta G^\circ_{r,\,298.15K}$ are the enthalpy and Gibbs free energy of reaction (1) at 298.15 K; $\Delta H^\circ_{f,\,H2O,\,298.15K}$ and $\Delta G^\circ_{f,\,H2O,\,298.15K}$

Table 2
Derived equilibrium constants for Reaction (1) at 0.1 MPa.

Humidity buffer	T (°C)	% RH	f^*_{H2O} (MPa)	ln K
NaBr	35.8 ± 0.2	54.32 ± 0.06	0.005951	−6.864 ± 0.020
KI	56.20 ± 0.2	63.62 ± 0.03	0.016541	−4.503 ± 0.019

Table 3
Derived thermodynamic parameters for Reaction (1) at 298.15 K and 0.1 MPa.

ΔG^0_r (kJ/mol)	ΔH^0_r(kJ/mol)	ΔS^0_r(J/mol·K)
20.436 ± 0.044	97.89 ± 0.69	259.8 ± 2.5

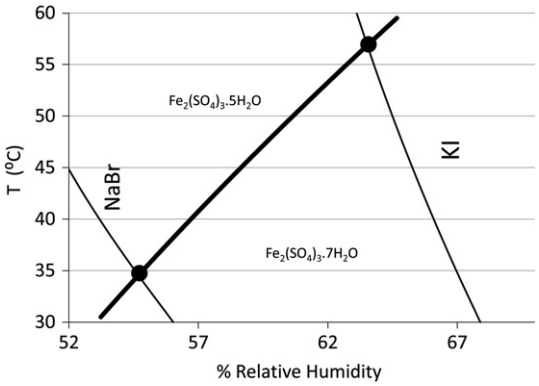

Fig. 5. The obtained phase boundary between kornelite and pentahydrated ferric sulfate at 0.1 MPa based on the thermodynamic parameters listed in Table 3. The dots represent equilibrium points at 56.2 and 35.8 °C where KI and NaBr humidity buffer curves intersect with 5w–7w phase boundary, respectively.

are the enthalpy and Gibbs free energy of formation from elements to water vapor at 298.15 K (Cox et al., 1989).

Based on the measured enthalpies of formation for pentahydrated ferric sulfate (Majzlan et al., 2006) and kornelite (Ackermann et al., 2009), the enthalpy change for each water of crystallization in the pentahydrated ferric sulfate and kornelite system should be -291 ± 3 kJ/mol. The enthalpy of reaction for the dehydration of kornelite to form $Fe_2(SO_4)_3 \cdot 5H_2O$ derived from our experiments is 97.9 ± 0.7 kJ/mol (Table 3). When counting the enthalpy of formation of water vapor to be -241.8 kJ/mol (Cox et al., 1989), the enthalpy change for each water molecule of crystallization in ferric sulfates is -290.8 ± 0.3 kJ/mol, which agrees, within experimental error, with the value calculated from the data of Majzlan et al. (2006) and Ackermann et al. (2009).

Based on our experimental results, the Gibbs free energy of reaction for the dehydration of kornelite to form $Fe_2(SO_4)_3 \cdot 5H_2O$ is 20.44 kJ/mol (Table 3). When counting the Gibbs free energy of formation of water vapor as -228.6 kJ/mol (Cox et al., 1989), the Gibbs free energy change for each water molecule of crystallization in ferric sulfates is -238.82 ± 0.02 kJ/mol. This value is very close to the value of -238.0 kJ/mol estimated by Hemingway et al. (2002) for hydrate sulfate salts in general, and to those values reported by Chou et al. (2002) for melanterite–rozenite (-238.34 kJ/mol) and chalcanthite–bonattite (-239.90 kJ/mol) equilibria, by Chou and Seal (2003a) for epsomite–hexahydrite equilibria (-238.73 kJ/mol), by Chou and Seal (2003b) for morenosite–retgersite equilibria (-237.44 kJ/mol), by Chou and Seal (2005a) for goslarite–bianchite equilibria (-238.23 kJ/mol), and by Chou and Seal (2005b) for bieberite–moorhouseite equilibria (-238.03 kJ/mol). Apparently, the valence difference in the cations does not significantly affect the $\Delta G^{\circ}_{xw,\ 298.15K}$ values.

6. Summary and conclusions

We have determined experimentally two separate points on the phase boundary of kornelite and pentahydrated ferric sulfate. Using these two points, we derived the thermodynamic parameters for the 7 W–5 W dehydration reaction. Based on these thermodynamic parameters, we further derived the phase boundary between kornelite and pentahydrated ferric sulfate in the 30–60 °C temperature range, and this is the first experimentally derived 7w–5w phase boundary at $T \leq 56$ °C. We have also developed a new methodology to prepare the hydrous ferric sulfate samples whereby the mass change caused by the adsorbed water can be distinguished from that caused by the dehydration or rehydration process.

This study was designed as the first step in an investigation of the phase diagram for the water–ferric sulfate system in the temperature range (≤ 50 °C) relevant to Mars. By nature, the phase boundary between kornelite and pentahydrate ferric sulfate occurs in the temperature range between 36 and 56 °C, which is higher than the ordinary temperature range at Mars surface in equatorial region (medium obliquity period). Thus, the applications of this finding for Mars are limited to the areas with hydrothermal activities (fumaroles). Based on our study of stability fields of five ferric sulfates (Wang et al., 2010), the phase boundaries among kornelite, ferricopiapite, rhomboclase, and paracoquimbite would occur in a lower temperature range, and will be the topics of future study. The thermodynamic parameters derived here will serve as reliable references for future phase boundary determination. This experimental method will be used in the future investigations of the phase diagrams including other ferric sulfates (ferricopiapite, rhomboclase and coquimbite) at $T \leq 50$ °C to enhance our understanding of the formation and the evolution history of Martian ferric sulfates.

Acknowledgments and disclaimer

We thank Jill D. Pasteris and Randy L. Korotev for their help on providing some essential experimental equipment. We thank Harvey Belkin and Rob Robinson of USGS for their critical reviews. We highly appreciate the constructive suggestions from Jeremy Fein and two anonymous reviewers for the improvement of our manuscript. We thank Randy L. Korotev for correcting the grammar errors of this manuscript. This study was supported by the Chinese Scholarship Council (to WGK) and two NASA Mars Fundamental Research projects (NNX07AQ34G and NNX10AM89G). The use of trade, product, industry, or firm names in this report is for descriptive purposes only and does not constitute endorsement by the U.S. Government.

References

Ackermann, S., et al., 2009. Thermodynamic and crystallographic properties of kornelite [$Fe_2(SO_4)_3 \cdot 7.75H_2O$] and paracoquimbite [$Fe_2(SO_4)_3 \cdot 9H_2O$]. American Mineralogist 94 (11–12), 1620–1628.

Baskerville, W.H., Cameron, F.K., 1935. Ferric oxide and aqueous sulfuric acid at 25 °C. The Journal of Physical Chemistry 39, 769–779.

Bell 3rd, J.F., et al., 2003. The Mars Exploration Rover Athena Panoramic Camera (Pancam) investigation. Journal of Geophysical Research 108 (E12), 8063.

Bishop, J.L., et al., 2009. Mineralogy of Juventae Chasma: sulfates in the light-toned mounds, mafic minerals in the bedrock, and hydrated silica and hydroxylated ferric sulfate on the plateau. Journal of Geophysical Research, Planets 114, E00D09.

Buckby, T., Black, S., Coleman, M.L., Hodson, M.E., 2003. Fe-sulphate-rich evaporative mineral precipitates from the Rio Tinto, southwest Spain. Mineralogical Magazine 67 (2), 263–278.

Chipera, S.J., Vaniman, D.T., Bish, D.L., 2007. The effect of temperature and water on ferric-sulfates. Lunar and Planetary Science XXXVIII abstract # 1409.

Chou, I.M., Seal, R.R., 2003a. Determination of epsomite-hexahydrite equilibria by the humidity-buffer technique at 0.1 MPa with implications for phase equilibria in the system $MgSO_4$—H_2O. Astrobiology 3 (3), 619–630.

Chou, I.M., Seal, R.R., 2003b. Acquisition and evaluation of thermodynamic data for morenosite–retgersite equilibria at 0.1 MPa. American Mineralogist 88 (11–12), 1943–1948.

Chou, I.M., Seal, R.R., 2005a. Determination of goslarite–bianchite equilibria by the humidity-buffer technique at 0.1 MPa. Chemical Geology 215 (1–4), 517–523.

Chou, I.M., Seal, R.R., 2005b. Acquisition and evaluation of thermodynamic data for bieberite–moorhouseite equilibria at 0.1 MPa. American Mineralogist 90 (5–6), 912–917.

Chou, I.M., Seal, R.R., 2007. Magnesium and calcium sulfate stabilities and the water budget of Mars. Journal of Geophysical Research, Planets 112 (E11), 10.

Chou, I.M., Seal, R.R., Hemingway, B.S., 2002. Determination of melanterite–rozenite and chalcanthite–bonattite equilibria by humidity measurements at 0.1 MPa. American Mineralogist 87 (1), 108–114.

Cox, J.D., Wagman, D.D., Medvedev, V.A., 1989. CODATA Key Values for Thermodynamics. Hemisphere, New York.

Farrand, W.H., Glotch, T.D., Rice, J.W., Hurowitz, J.A., Swayze, G.A., 2009. Discovery of jarosite within the Mawrth Vallis region of Mars: implications for the geologic history of the region. Icarus 204 (2), 478–488.

Freeman, J.J., Wang, A., Ling, Z.C., 2009. Ferric sulfates on mars: mission observations and laboratory investigations. Lunar and Planetary Science Conference XL, abstract #2284.

Greenspan, L., 1977. Humidity fixed points of binary saturated aqueous solutions. Journal of Research of the National Bureau of Standards. Section A. Physics and Chemistry B1A, 89–96.

Haar, L., Gallagher, J.S., Kell, G.S., 1984. NBS/NRC Steam Tables: Thermodynamic and Transport Properties and Computer Programs for Vapor and Liquid States of Water in SI Units. Hemisphere, Washington, DC. 320 pp.

Hemingway, B.S., Seal 2nd, R.R., Chou, I.-M., 2002. Thermodynamic data for modeling acid-mine drainage problems. Part I. Selected soluble iron-sulfate minerals. U.S. Geol. Surv. Open-File Rep. 02, 161, 13 pp.

Jambor, J.I., Nordstrom, D.K., Alpers, C.N., 2000. Metal-sulfate salts from sulfide mineral oxidation. Sulfate minerals — crystallography. Geochemistry and Environmental Significance 40, 303–350.

Jerz, J.K., Rimstidt, J.D., 2003. Efflorescent iron sulfate minerals: paragenesis, relative stability, and environmental impact. American Mineralogist 88 (11–12), 1919–1932.

Johnson, J.R., et al., 2007. Mineralogic constraints on sulfur-rich soils from Pancam spectra at Gusev crater, Mars. Geophysical Research Letters 34 (13), 6.

Kieffer, H.H., et al., 1977. Thermal and albedo mapping of Mars during the Viking primary mission. Journal of Geophysical Research 82 (28), 4249–4291.

Klingelhöfer, G., et al., 2003. Athena MIMOS II Mössbauer spectrometer investigation. Journal of Geophysical Research 108 (E12), 8067.

Klingelhöfer, G., et al., 2004. Jarosite and hematite at Meridiani Planum from opportunity's Mössbauer spectrometer (no.5702 (03 DEC 2004)) Science 306, 1740–1745.

Lichtenberg, K.A., et al., 2010. Stratigraphy of hydrated sulfates in the sedimentary deposits of Aram Chaos, Mars. Journal of Geophysical Research 115, E00D17.

Ling, Z.C., Wang, Alian, 2010. A systematic spectroscopic study of eight hydrous ferric sulfates relevant to Mars. Icarus 209 (2), 422–433.

Ling, Z.C., et al., 2008. A systematic Raman, mid-IR, and Vis–NIR spectroscopic study of ferric sulfates and implications for sulfates on Mars. Lunar and Planetary Science Conference XXXIX Abstract # 1463.

Majzlan, J., Botez, C., Stephens, P.W., 2005. The crystal structures of synthetics Fe—Fe—$_2(SO_4)\cdot 5H_2O$ and the type specimen of lausenite. American Mineralogist 90 (2–3), 411–416.

Majzlan, J., Navrotsky, A., McCleskey, R.B., Alpers, C.N., 2006. Thermodynamic properties and crystal structure refinement of ferricopiapite, coquimbite, rhomboclase, and Fe—$_2(SO_4)_3\cdot 5H_2O$. European Journal of Mineralogy 18 (2), 175–186.

Merwin, H.E., Posnjak, E., 1937. Sulfate incrustations in the copper queen mine, Bisbee, Arizona. American Mineralogist 22, 567–571.

Morris, R.V., et al., 2006. Mossbauer mineralogy of rock, soil, and dust at Gusev crater, Mars: Spirit's journey through weakly altered olivine basalt on the plains and pervasively altered basalt in the Columbia Hills. Journal of Geophysical Research, Planets 111 (E2), 28.

Morris, R.V., et al., 2008. Iron mineralogy and aqueous alteration from Husband Hill through Home Plate at Gusev Crater, Mars: results from the Mossbauer instrument on the Spirit Mars Exploration Rover. Journal of Geophysical Research, Planets 113 (E12), 43.

Nordstrom, D.K., Alpers, C.N., 1999. Negative pH, efflorescent mineralogy, and consequences for environmental restoration at the Iron Mountain Superfund site, California. Proceedings of the National Academy of Sciences of the United States of America 96 (7), 3455–3462.

Nordstrom, D.K., Alpers, C.N., Ptacek, C.J., Blowes, D.W., 2000. Negative pH and extremely acidic mine waters from Iron Mountain, California. Environmental Science & Technology 34 (2), 254–258.

Posnjak, E., Merwin, H.E., 1922. The system, Fe_2O_3—SO_3—H_2O. Journal of the American Chemical Society 44, 1965–1994.

Roach, L.H., Mustard, J.F., Murchie, S.L., Bishop, J.L., Weitz, C.M., Knudson, A.T., Bibring, J.-P., Pelkey, S.M., Ehlmann, B.L., the CRISM Science Team, 2007. Magnesium and iron sulfate variety and distribution in East Candor and Capri Chasma, Valles Marineris. 7th Int. Conf. on Mars. Abstract # 3223.

Robinson, P.D., Fang, J.H., 1973. Crystal structures and mineral chemistry of hydrated ferric sulfates. III. The crystal structure of kornelite. American Mineralogist 58, 535–539.

Schofield, J.T., et al., 1997. The Mars Pathfinder Atmospheric Structure Investigation/Meteorology (ASI/MET) experiment. Science 278 (5344), 1752–1757.

Smith, M.D., et al., 2004. First atmospheric science results from the Mars Exploration Rovers Mini-TES. Science 306 (5702), 1750–1753.

Spanovich, N., et al., 2006. Surface and near-surface atmospheric temperatures from the Mars Exploration Rover landing sites. Icarus 180, 314–320.

Tosca, N.J., Smirnov, A., McLennan, S.M., 2007. Application of the Pitzer ion interaction model to isopiestic data for the $Fe_2(SO_4)_3$—H_2SO_4—H_2O system at 298.15 and 323.15 K. Geochimica et Cosmochimica Acta 71 (11), 2680–2698.

Wang, A., Ling, Z.C., 2011. Ferric sulfates on Mars: A combined mission data analysis of salty soils at Gusev crater and laboratory experimental investigations. Journal of Geophysical Research, Planets 116 (E0), 22.

Wang, A., Freeman, J.J., Greenhagen, B.T., Jolliff, B.L., 2005. Raman Spectra of Hydrated Mg & Ca-sulfates and Field Test of MMRS. Salt Lake City Annual Meeting by The Geological Society of America.

Wang, A., Freeman, J.J., Jolliff, B.L., Chou, I.M., 2006. Sulfates on Mars: a systematic Raman spectroscopic study of hydration states of magnesium sulfates. Geochimica et Cosmochimica Acta 70 (24), 6118–6135.

Wang, A., et al., 2008a. Light-toned salty soils and coexisting Si-rich species discovered by the Mars Exploration Rover Spirit in Columbia Hills. Journal of Geophysical Research, Planets 113 (E12), 35.

Wang, A., Ling, Z., Freeman, J.J., 2008b. Ferric sulfates on Mars: surface explorations and laboratory experiments. EOS Transactions AGU 89, 44A–A Fall Meeting Supplement, abstract #.

Wang, A., Ling, Z., Freeman, J.J., 2010. Stability fields and phase transition pathways of ferric sulfates in 50 °C to 5 °C temperature range. Lunar and Planetary Science Conference XLI Abstract # 1463.

Williams, A.P., 1990. Oxide Zone Geochemistrysecond ed. Horwood, New York.

Wirth, F., Bakke, B., 1914. Untersuchung über Ferrisulfate. Darstellung und Eigenschaften der verschiedenen normalen, basischen und sauren Ferrisulfate. Löslichkeits- und Stabilitatsverhaltnisse in Wasser und Schwefelsäure Kristallisationsgang. Zeitschrift fur Anorganische Chemie 87, 13–46.

Xu, W.Q., Tosca, N.J., McLennan, S.M., Parise, J.B., 2009. Humidity-induced phase transitions of ferric sulfate minerals studied by in situ and ex situ X-ray diffraction. American Mineralogist 94 (11–12), 1629–1637.